Spectrochimica Acta Part A: Molecular and Biomolecular Spectroscopy 364 (2027) 128536

Contents lists available at ScienceDirect

Spectrochimica Acta Part A:
Molecular and Biomolecular Spectroscopy

journal homepage: www.journals.elsevier.com/spectrochimica-acta-part-a-molecular-and-biomolecular-spectroscopy

Pillararene-based fluorescence indicator displacement assays for the ratiometric and turn-on detection of ATP

Etelka Kiss [a,b], Dávid Mester [a,c,d], Dóra Hessz [a], Ervin Kovács [b,e], Krisztina László [a], Miklós Kubinyi [a,*]

[a] Department of Physical Chemistry and Materials Science, Faculty of Chemical Technology and Biotechnology, Budapest University of Technology and Economics, Műegyetem rkp. 3, H-1111 Budapest, Hungary
[b] BrainVisionCenter Research Institute, Liliom u. 43-45, H-1094 Budapest, Hungary
[c] MTA-BME Lendület Quantum Chemistry Research Group, Budapest University of Technology and Economics, Műegyetem rkp. 3, H-1111 Budapest, Hungary
[d] ELKH-BME Quantum Chemistry Research Group, Budapest University of Technology and Economics, Műegyetem rkp. 3, H-1111 Budapest, Hungary
[e] Institute of Materials and Environmental Chemistry, HUN-REN Research Centre for Natural Sciences, Budapest, Magyar tudósok körútja 2, H-1117 Budapest, Hungary

HIGHLIGHTS

- Acidic dissociation of HPTS is promoted on complexation with cationic pillar[6]arene.
- HPTS – cationic pillar[6]arene complex acts as a fluorescent ratiometric IDA for ATP.
- Turn-on ATP sensor was made exploiting the FRET quenching of HPTS by reduced GO.
- Broad linear range of turn-on ATP sensor in 1% human serum.
- Structures of host-guest complexes determined by NMR and theoretical calculations.

GRAPHICAL ABSTRACT

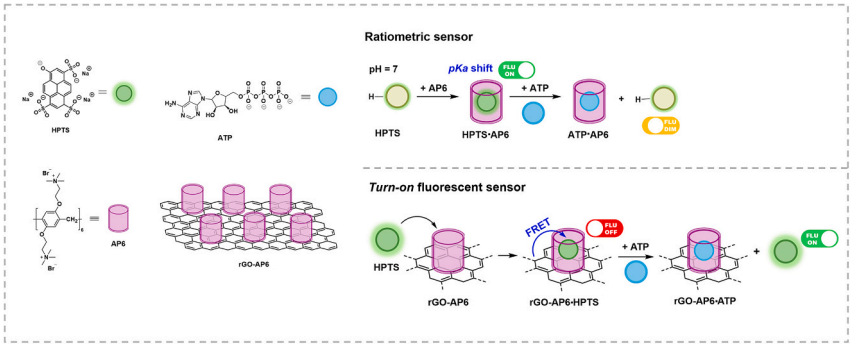

ARTICLE INFO

Keywords:
Fluorescence indicator displacement (FID) assay
Turn-on fluorescent probe
Förster resonance energy transfer (FRET)
Reduced graphene oxide
Nucleotide sensor
HPTS (Pyranine)

ABSTRACT

For ATP detection, indicator displacement assays with multicationic macrocyclic hosts and anionic fluorescent dye guests represent an intuitive design strategy. However, such systems typically exhibit *turn-off* responses. For biological samples with strong background- and autofluorescence, ratiometric or *turn-on* signaling is preferred, which requires more sophisticated assay architectures. In the present work, the host-guest complexation of fluorescent pH indicator dye trisodium 8-hydroxypyrene-1,3,6-trisulfonic acid (HPTS) with a cationic ammonium-pillar[6]arene (AP6) was employed in the design of indicator displacement assays featuring two distinct detection modes for the fluorescent sensing of nucleotide ATP. In the first approach, AP6-assisted deprotonation of HPTS enabled the development of a colorimetric and a fluorescent ratiometric assay. In the second strategy, fluorescence *turn-on* sensing was achieved by exploiting the FRET-type quenching of HPTS fluorescence by AP6-modified reduced graphene oxide (rGO-AP6). Both sensing platforms demonstrated high selectivity toward ATP over structurally similar nucleotides and other biologically relevant anions, a broad dynamic range and a low limit of detection. The performance of the *turn-on* ATP sensor was validated in the

* Corresponding author.
E-mail address: kubinyi.miklos@vbk.bme.hu (M. Kubinyi).

https://doi.org/10.1016/j.saa.2026.128536
Received 4 June 2026; Received in revised form 27 July 2026; Accepted 31 July 2026
Available online 2 August 2026

complex biological matrix of human serum, demonstrating its applicability for practical bioanalytical applications.

1. Introduction

Adenosine triphosphate (ATP) functions as the "energy currency" of the cell, plays a central role in cellular energy metabolism, the synthesis and degradation of biomolecules, membrane transport processes and DNA replication. Abnormal ATP concentrations have been associated with several diseases, including ischemia, Parkinson's and Alzheimer's disease [1], cancer [2] and hypoglycemia.

Several methods have been developed for the detection and quantification of nucleoside polyphosphates, like capillary electrophoresis [3], high-performance liquid chromatography [4], aptamer-based assays [5–8], luciferase-based bioluminescence methods [9], nanomaterials [10] and synthetic fluorescent sensors. The most popular and commercialized method to quantify ATP is the luciferin/luciferase system, which requires cell lysis, the extraction of ATP from the intact cells [11]. Synthetic fluorescent probes offer the advantage of enabling live-cell imaging, without the need for cellular transfection [12]. Fluorescent probes include direct cationic probes and fluorescent indicator displacement (FID) assays. In the case of direct probes, the fluorophore interacts with ATP through either one or two mechanisms (electrostatic interactions with the phosphate chain, π-π stacking with the adenosine base, or complexation to the vicinal diol of the ribose ring [13,14]), which often results in limited selectivity, low binding affinity and/or may lead to aggregation [15].

An advantage FID assays offer is that the macrocyclic host component usually engages with the fluorophore/target analyte through multiple synergistic effects (multiple electrostatic, π-π and hydrophobic interactions), resulting in improved sensitivity, selectivity and a larger signal change. Several indicator displacement assays have been designed for the detection of nucleotides and inorganic phosphates [16–18], including ATP [19–22]. However, most of these systems function as colorimetric or fluorescence *turn-off* sensors.

As fluorescent nucleotide sensors are applied in biological samples, which usually have strong background interference, sensors affording ratiometric measurement and sensors with *turn-on* response are greatly advantageous.

In this study, three types of sensors have been developed for ATP detection: a colorimetric ratiometric, a fluorescent ratiometric and a fluorescent *turn-on* sensor. All three systems are based on supramolecular complexes of cationic ammonium-pillar[6]arene (AP6) as the host component, and commercially available anionic dye, trisodium-1,3,6-trisulfonic acid (HPTS, a.k.a. Pyranine) as the guest component (Scheme 1. A). In addition to creating efficient new chemosensors for ATP detection, our aim has been to compare the performance of the sensors with different detection modes. Our colorimetric and fluorescent ratiometric sensors utilize the pK_a shift observed in the HPTS·AP6 complex, resulting in distinct changes in its absorption spectra and fluorescent properties (Scheme 1. B). For the fluorescent *turn-on* assay, AP6 was grafted onto the surface of reduced graphene oxide via electrostatic interactions, forming adduct rGO-AP6 [23]. The adduct quenches the fluorescence of bound HPTS molecules through a process primarily attributed to Förster resonance energy transfer (FRET). In the presence of ATP, HPTS is displaced from the rGO-AP6 surface, and its fluorescence is regenerated (Scheme 1. C).

Several fluorescent ATP sensors utilizing the FRET effect have been reported in the literature, mainly protein-based and aptamer-based

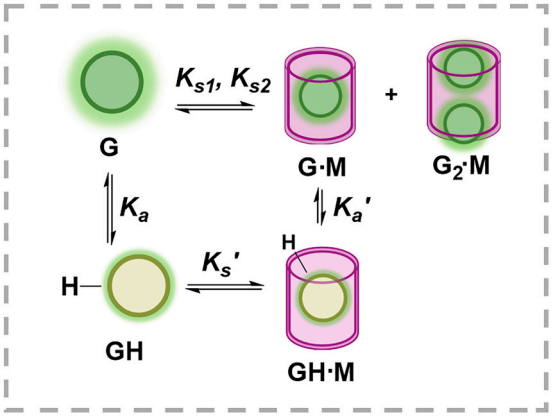

Scheme 2. The cyclic reaction process of HPTS complexation; G denotes tetraanionic HPTS, GH the trianionic HPTS species, while M represents AP6 macrocyclic host.

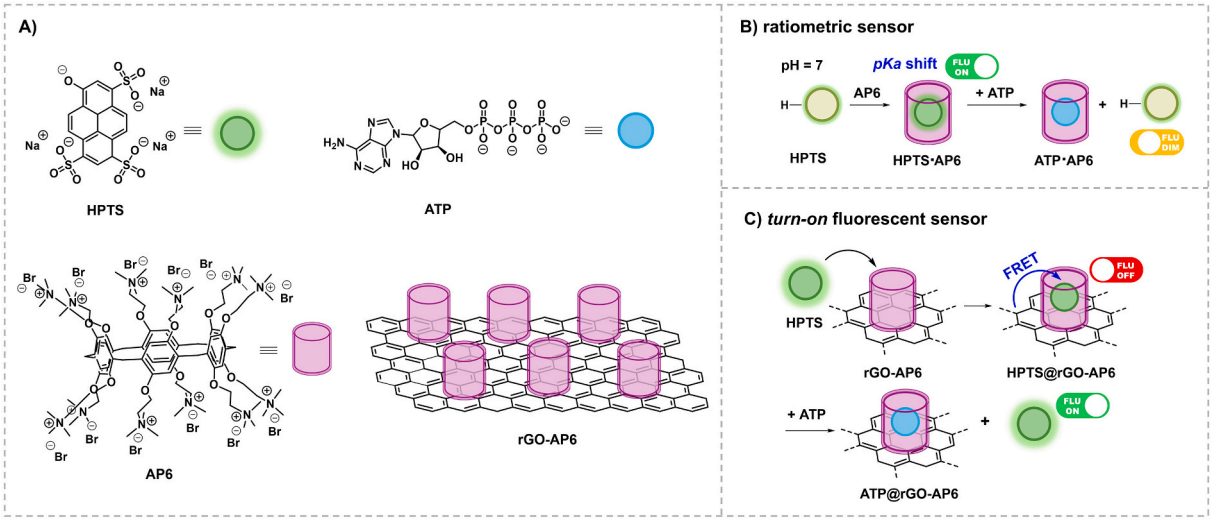

Scheme 1. A) Structures and symbols of fluorescent dye (HPTS), cationic pillar[6]arene (AP6), nanocomposite rGO-AP6 and analyte ATP; B) working concept of the colorimetric and ratiometric fluorescent ATP-sensors; C) working concept of the *turn-on* fluorescent ATP-sensor.

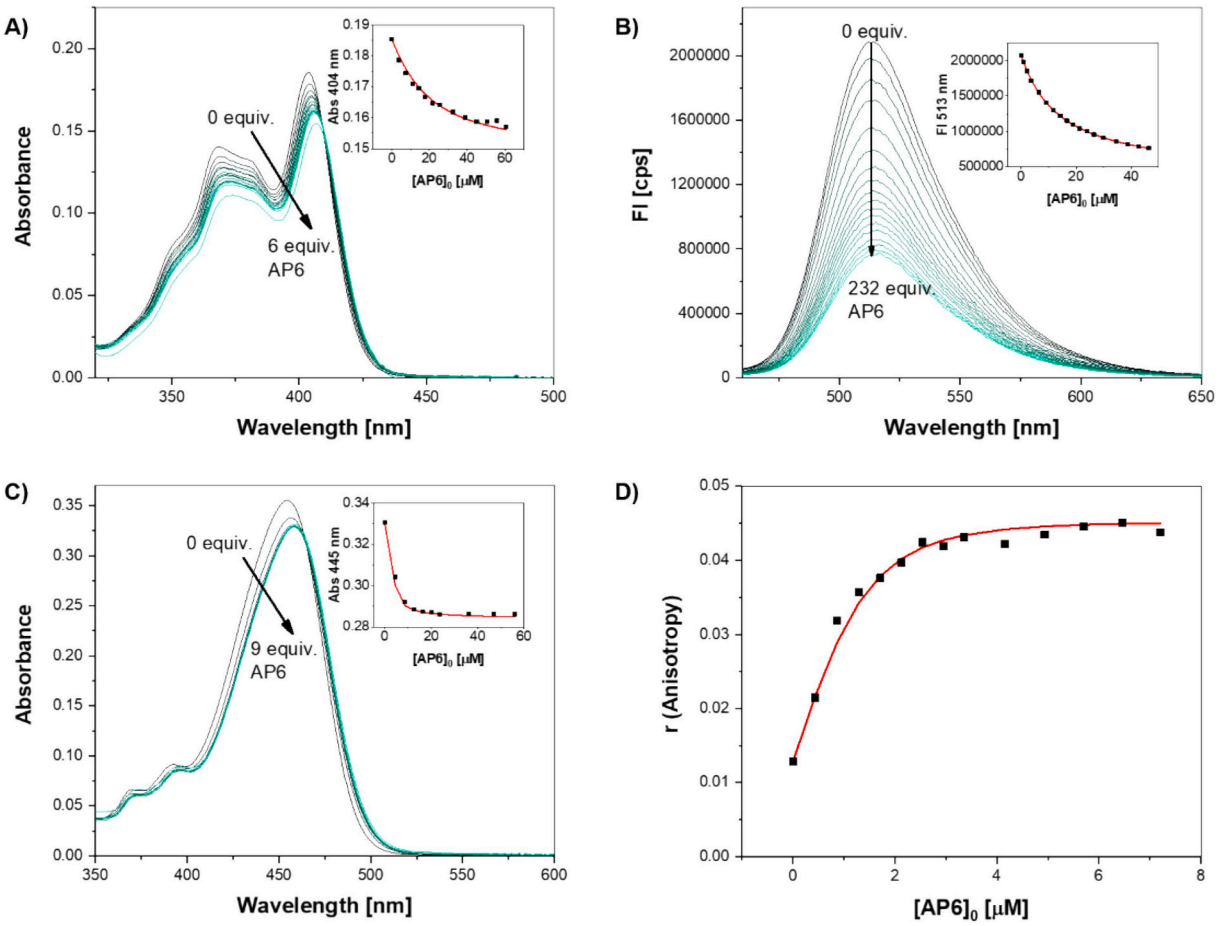

Fig. 1. (A) UV–visible absorption spectra of 10^{-5} M HPTS +0–6 equiv. AP6 mixtures at pH = 4.5 (Britton-Robinson buffer); (B) Fluorescence emission spectra of $2{\cdot}10^{-7}$ M HPTS +0–232 equiv. of AP6 mixtures at pH = 4.5 (Britton-Robinson buffer), λ_{exc} = 410 nm; (C) UV–visible absorption spectra of $2{\cdot}10^{-5}$ M HPTS +0–9 equiv. of AP6 mixtures at pH = 10.2 (CAPS buffer); (D) Fluorescence anisotropy (r) vs AP6 concentration in $2{\cdot}10^{-6}$ M HPTS +0–2.3 equiv. of AP6 mixtures at pH = 10.2 (CAPS buffer), λ_{exc} = 465 nm; the insets show the absorbance/fluorescence intensity changes at given wavelength, the red lines show the fit of the applied model. (For interpretation of the references to color in this figure legend, the reader is referred to the web version of this article.)

Table 1
Binding constants of 1:1 and 2:1 HPTS-AP6 complexes.

Host-guest system	Method	Medium	K_s', K_{s1} [M^{-1}]	K_{s2} [M^{-1}]
GH + AP6	Absorption spectroscopy	4.5 pH Britton-Robinson buffer (ionic strength 0.04 M)	$(7.15 \pm 0.77){\cdot}10^4$	–
	Fluorescence spectroscopy	4.5 pH Britton-Robinson buffer (ionic strength 0.04 M)	$(7.11 \pm 0.08){\cdot}10^4$	–
G^- + AP6	Absorption spectroscopy	10.2 pH CAPS buffer (ionic strength 0.01 M)	$(3.60 \pm 0.79){\cdot}10^6$	$(8.9 \pm 7.9){\cdot}10^5$
	Fluorescence anisotropy	10.2 pH CAPS buffer (ionic strength 0.01 M)	$(3.44 \pm 1.0){\cdot}10^6$	$(9.9{\pm}0.95){\cdot}10^5$

sensors [24–27]. However, to our knowledge, no FID assay based on the interaction of a fluorescent dye (acting as FRET-donor) and macrocycle grafted onto a nanoparticle (acting as FRET-acceptor) with selectivity for ATP has been reported so far.

Our study encompasses the systematic design and characterization of the various type ATP sensors, the description of the structures of the HPTS-AP6 supramolecular complexes and the testing of the FRET-type sensor in human blood serum.

2. Materials and methods

2.1. Materials

AP6 was synthesized as described in Ref. [28]. First, a pillar[6]arene perfunctionalized with 2-bromoethoxy groups (BrP6) was prepared by the condensation of 1,4-bis(2-bromoethoxy)-benzene and para-formaldehyde. AP6 was obtained then by reacting BrP6 with trimethylamine in large excess.

The synthesis of graphene oxide followed an improved Hummers method [29]. The graphite powder used in the synthesis was purchased from the Graphite Týn, Týn nad Vltavou chemical company (Czech Republic) (particle size is <63 μm according to the manufacturer). A detailed characterization of graphene oxide can be found in Ref. [30]. rGO-AP6 was synthesized according to the procedure reported in Ref. [31]. A mixture of 0.5 mg/ml graphene oxide aqueous suspension and 0.5 mg/ml pillar[6]arene (AP6) was ultrasonicated for 10 min, then stirred for 4 h (1000 rpm, 24 °C). 2 ml of 1 M sodium-hydroxide was added, then the mixture was stirred for 4 h again at 90 °C. The brown suspension turned black. The cooled mixture was centrifuged, washed, then dried at 70 °C for 18 h.

Buffer component Tris was purchased from ThermoFisher Scientific, HEPES and Bis-Tris was purchased from Merck. Hydrochloric acid and

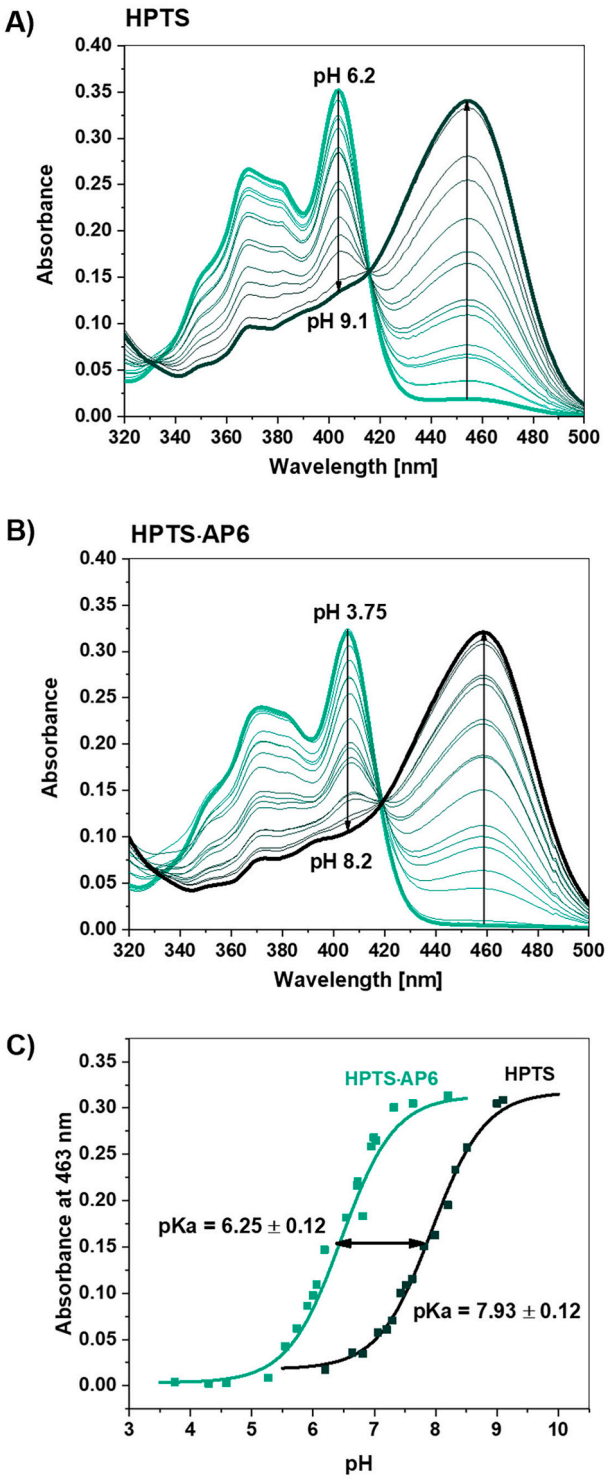

Fig. 2. (A) Absorption spectra of HPTS ($2{\cdot}10^{-5}$ M) in Tris buffer mixtures (pH 6.2–9.1); (B) Absorption spectra of HPTS ($2{\cdot}10^{-5}$ M) and AP6 (5.2 equiv.) in Bis-Tris (pH 4.6–7) and Tris buffer mixtures (pH 7.2–8.2); (C) Absorbance changes at 463 nm, the isosbestic point for deprotonated HPTS and its AP6 complex vs pH; connected lines show the fits of the applied models.

sodium hydroxide were used to set the pH of the buffer mixtures. Fluorescent dye HPTS was purchased from Alfa Aesar and used without further purification. MilliQ water was used in all experiments.

2.2. Methods

2.2.1. Spectroscopic experiments

UV–Vis absorption spectra were recorded on an Agilent 8453 single-beam spectrophotometer.

Fluorescence emission, excitation and anisotropy spectra were measured on an Edinburgh Instruments FS5 spectrofluorometer. When measuring fluorescence emission spectra of samples containing suspensions of rGO-AP6, the polarizers of the instrument were set to orthogonal positions, and cutoff optical filters were employed to avoid light scattering from the colloidal material.

Fluorescence anisotropy was measured automatically in the range 510–520 nm, and average anisotropies (r) were determined.

^{1}H NMR spectra were measured on a 500 MHz Varian NMR narrow bore spectrometer with 1 s relaxation times. The spectra of protonated HPTS were studied in DCl + D_2O solution (pD = 2), deprotonated HPTS spectra were measured in NaOD + D_2O solution (pD = 12). The sodium salt of 3-(trimethylsilyl)-1-propanesulfonic acid (DSS) was added as reference.

2.2.2. Computational methods

For the theoretical calculations, conformational analysis was carried out using the CREST algorithm [32] at the semiempirical GFN2-xTB level of theory [33]. The complex structures were generated using an in-house script and the Autodock Vina package [34]. The lowest-energy geometries were selected and further optimized using the Gaussian 09 software package [35] at the ωB97X-D/def2-SVP level of theory [36]. Single-point energy calculations were performed at the ωB97X-D/def2-SVPD level of theory. Both semiempirical and DFT calculations were carried out using water as the solvent.

2.2.3. Determination of equilibrium constants

The acidic dissociation constant K_a of the HPTS dye was determined from its absorption spectra measured in the 6.2–9.1 pH range in Tris buffers. A global fitting was made to the experimental spectra with pK_a as the adjustable parameter. The pK_a value for the HPTS·AP6 complex was determined in a similar manner, the samples were HPTS solutions of different pH values in Bis-Tris and Tris buffers to which 5.2 eq. AP6 was added.

The binding constant for the AP6 complex of protonated HPTS, K_s', was determined both by absorption and fluorescence spectroscopy. The samples were prepared in Britton-Robinson buffer solutions of pH = 4.5, with constant dye concentration and increasing pillar[6]arene concentrations.

In the interaction of deprotonated HPTS with AP6, complexes of 1:1 and of 2:1 (dye:pillararene) stoichiometry were observed. The binding constants K_{s1} and K_{s2} were determined both by absorption spectroscopy and by fluorescence anisotropy measurements in CAPS buffer solutions of pH = 10.2. The binding constants were obtained by global fittings to the experimental data.

The indicator displacement experiments were carried out in HEPES buffer solutions, the pH and the concentration of AP6 were optimization parameters. The spectra obtained from the HPTS-AP6-ATP ternary systems afforded the calculation of the binding constant for the ATP·AP6 complex by global fitting.

The algorithms used for the determination of the acidic dissociation constants and binding constants by global fitting are described in detail in the SI.

3. Results

3.1. Reactions in HPTS – AP6 system

3.1.1. Scheme of reactions

The scheme of reactions observed in the HPTS – AP6 system is presented in Scheme 2. The protonation of the hydroxyl group of HPTS, the

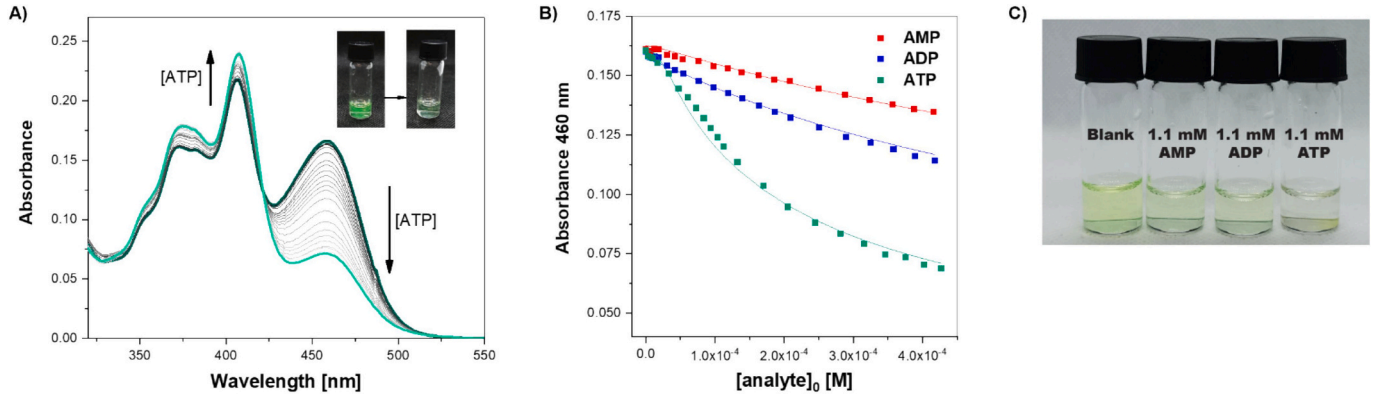

Fig. 3. (A) Absorption spectra of HPTS ($2{\cdot}10^{-5}$ M) – AP6 ($1.5{\cdot}10^{-5}$ M) system in the presence of ATP nucleotide; the inset shows the color changes observed after the addition of ATP (HEPES buffer solution, pH = 7); (B) Absorbance changes at 460 nm detected at the addition of ATP, ADP and AMP nucleotides, scatter plot – measured data, line plot – fitted functions; (C) photographs of HPTS·AP6 in presence of 1.1 mM of the nucleotides under visible light.

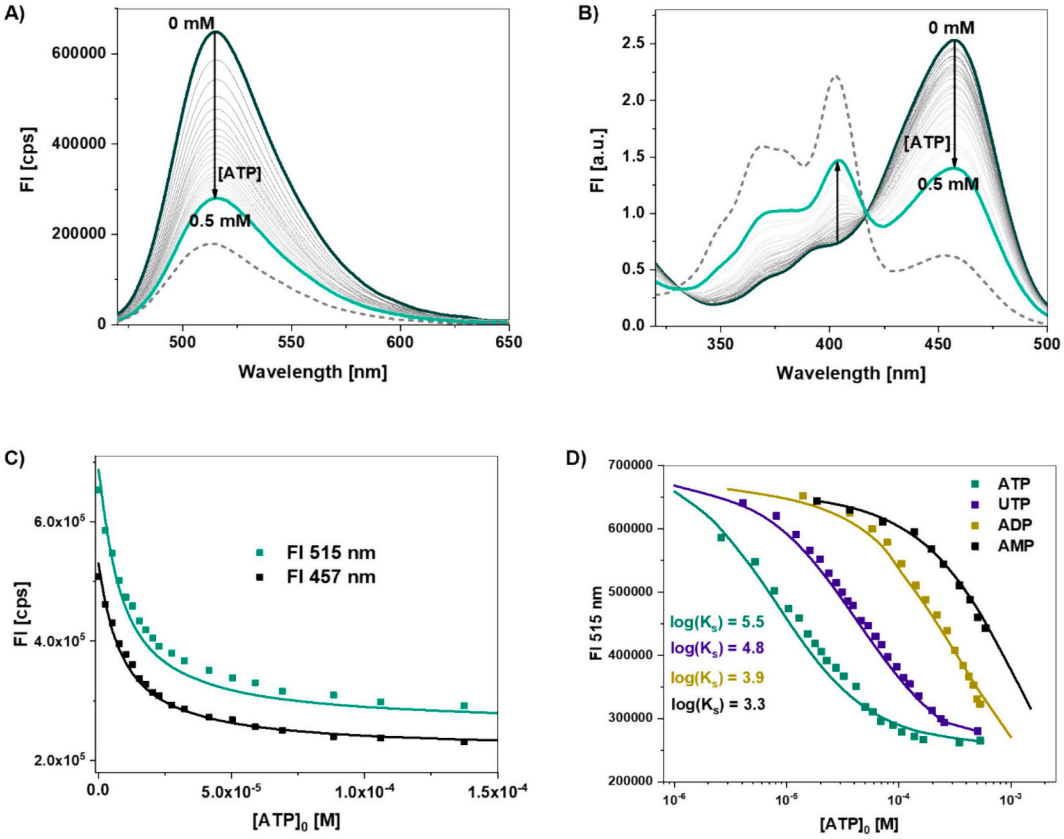

Fig. 4. (A) Fluorescence emission spectra of HPTS·AP6 ($2{\cdot}10^{-6}$ M HPTS $+2.2{\cdot}10^{-6}$ M AP6) in the presence of 0–0.5 mM of ATP, $\lambda_{exc} = 457$ nm; (B) Fluorescence excitation spectra of HPTS·AP6 in the presence of 0–0.5 mM of ATP, $\lambda_{em} = 515$ nm; (C) Fluorescence intensities at 515 nm (from A) and 457 nm (from B) vs the initial concentration of ATP; (D) Fluorescence responses of the assay vs concentration of ATP (semi-logarithmic scale) measured at increasing concentrations of ATP, UTP, ADP and AMP; pH = 7, HEPES buffer; scatter plot – measured data, line plot – fitted function.

complexation of HPTS, the protonation of the HPTS·AP6 complex and the complexation of protonated HPTS are equilibrium reactions forming a cyclic reaction scheme. In HPTS – AP6 mixtures with HPTS excesses, 2:1 dye-pillararene complex has also been detected. The design of the ATP sensors required the knowledge of the equilibrium constants characterizing the HPTS – AP6 system.

3.1.2. Binding constants

The binding of the protonated form of HPTS to AP6 was studied in Britton-Robinson buffer of pH = 4.5, whereas the binding of the deprotonated dye to the pillararene was studied in pH = 10.2 CAPS buffer. Considering the pK_a values of free HPTS and its AP6 complex at pH 4.5 (see section 3.1.3), the dissociation of these species was negligible, whereas at pH 10.2, the dye and its complex were practically fully dissociated. The association constant of protonated HPTS (GH) with pillararene AP6 (M)

$$K_s' = \frac{[GH{\cdot}M]}{[GH][M]} \tag{1}$$

was determined both by absorption and fluorescence spectroscopy. The

Table 2
Binding constants of the ATP·AP6 and rGO-AP6·ATP complexes, determined by indicator displacement experiments.

Assay	Analyte	K_b $[M]^{-1}$	Method
AP6 + HPTS	ATP	$2.94 \cdot 10^5$	Absorption spectroscopy – colorimetric
		$3.55 \cdot 10^5$	Fluorescence spectroscopy – *turn-off*
		$3.18 \cdot 10^5$	Fluorescence spectroscopy – ratiometric
rGO-AP6 + HPTS	ATP	$2.68 \cdot 10^5$	Fluorescence spectroscopy – *turn-on*

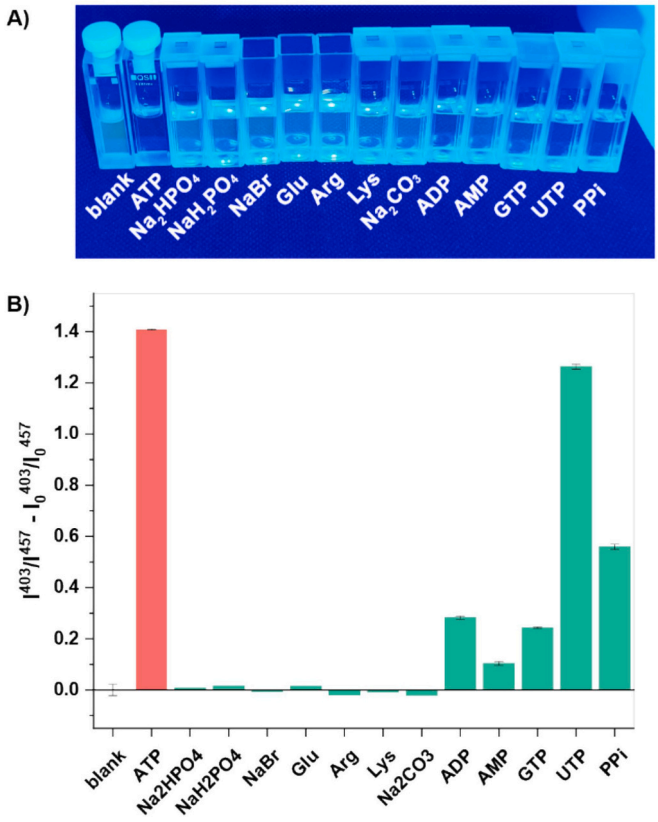

Fig. 5. (A) Photograph of the HPTS·AP6 assay recorded under 460 nm LED irradiation and (B) fluorescence response toward 0.5 mM ATP compared with nucleotides, amino acids and naturally occurring anions, $\lambda_{em} = 515$ nm, pH = 7; the composition of the complex is $2 \cdot 10^{-6}$ M HPTS and 1.1 equiv. of AP6; error bars represent standard deviation from 2 parallel measurements.

details of this calculation are presented in detail in Section S1 of the SI.

For the absorption measurements, 0–6 equiv. of AP6 was added in small amounts to a solution where the concentration of HPTS was kept constant (Fig. 1. A). The same experimental conditions were applied for the fluorescence studies, where 0–232 equiv. of AP6 was added step by step to a HPTS solution, and the emission spectra were recorded (Fig. 1. B). The excitation wavelength was chosen as the isosbestic point of the free HPTS dye (GH) and the complex (GH·M) – this way, the fluorescence spectra were not affected by the different absorption coefficients of the dye and its complex. The binding isotherm in Fig. 1. A reflects a typical 1:1 equilibrium binding model: the signal shows linear dependence at low pillararene concentrations and approaches a plateou when close to saturation. In the titration experiment illustrated in Fig. 1. B, AP6 was added to the solution of HPTS in high excesses. As follows from Eqs. (S2)–(S5) for the range $[M]_0 \gg [G]_0$, the binding isotherm has a closely hyperbolic shape. The binding constant values obtained by global fitting to the absorption and fluorescence emission spectra are presented in Table 1.

Upon the addition of AP6 to the deprotonated HPTS dye (G), the absorption and fluorescence emission spectra exhibited only minor changes. The absorption spectra are shown in Fig. 1. C. As the AP6·HPTS complex is significantly larger than the free HPTS tetraanion, and therefore the fluorescence anisotropy of the mixture would increase with the addition of AP6, fluorescence anisotropy was applied as a supplementary tool to absorption spectroscopy to study the binding of deprotonated HPTS and AP6 (Fig. 1. D).

The molar ratio plots of the absorbance and the fluorescence anisotropy data for mixtures of deprotonated HPTS and AP6 (Fig. S1) suggest a 2:1 as well as a 1:1 host-guest binding.

The values of the binding constants

$$K_{s1} = \frac{[G \cdot M]}{[M][G]} \tag{2}$$

$$K_{s2} = \frac{[G_2 \cdot M]}{[G][G \cdot M]} \tag{3}$$

determined by least-squares global fitting to the absorption spectra and to the average anisotropies are presented in Table 1.

The binding constants obtained from the absorption and fluorescence spectroscopic data are in close agreement. The AP6 host binds the OH-deprotonated form of the HPTS guest much stronger than its protonated form. The ratio of the two binding constants characterizing the complexation of the dissociated dye K_{s1}/K_{s2} is ≈ 4, indicating that the binding of the second guest is non-cooperative [37].

3.1.3. Acidic dissociation constants

Due to the preferential stabilization of the deprotonated form of HPTS in the complex of AP6, a significant downward shift of the dye pK_a has been expected on complexation.

First, the acidic dissociation constant of the free HPTS dye was determined from the absorption spectra of its $2 \cdot 10^{-5}$ M solutions with pH ranging from 6.2 to 9.1 (Fig. 2. A).

The acidic dissociation constant of the HPTS·AP6 complex was obtained by global fitting to the absorption spectra of HPTS – AP6 mixtures, the pH was varied in the 4.6–8.2 range. In the evaluation of the spectra, it was assumed that deprotonated HPTS exists in its fully complexed form, however, due to the lower binding constant of protonated HPTS with AP6, a fraction of the dye remains in the uncomplexed state, which fact must be considered when calculating the acidic dissociation constant of the complex. Details of this calculation are presented in Section S2 of the SI.

The global fittings yielded $pK_a = 7.93$ for HPTS and 6.25 for the HPTS·AP6 complex (Fig. 2. C). Thus, the acidic dissociation of HPTS was promoted significantly by its coordination to the cationic pillararene.

It follows from the formulae of the binding constants and acidic dissociation constants in the cyclic reaction scheme that they are related as

$$\frac{K_s}{K_s'} = \frac{K_a'}{K_a} \tag{4}$$

Substituting the corresponding values in Eq. 4 (only K_{s1} in case of the deprotonated HPTS),

$$\frac{3.44 \cdot 10^6}{7.11 \cdot 10^4} \approx 48 \approx \frac{10^{-6.25}}{10^{-7.93}}$$

The matching values of the calculated ratios further support the validity of the employed fitting models.

3.2. Displacement assays

The working principles of HPTS·AP6 and HPTS@rGO-AP6 indicator displacement assays are illustrated in Scheme 1. B) and C).

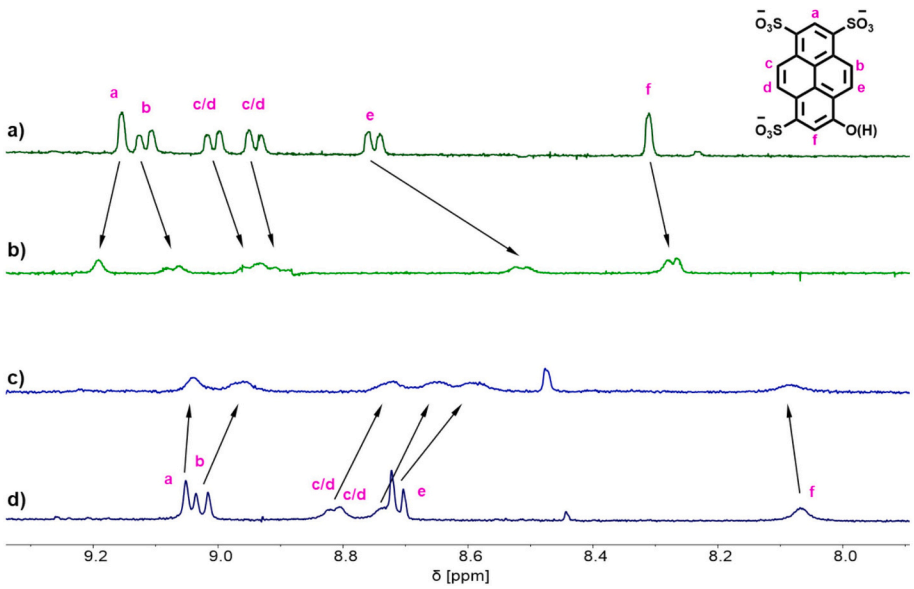

Fig. 6. Partial ^{1}H NMR spectra (500 MHz, 295 K, D_2O) of 2 mM HPTS (pD = 2) (a), a 1:1 mixture of 2 mM HPTS and AP6 (pD = 2) (b), a 1:1 mixture of 2 mM HPTS and AP6 (pD = 12) (c), and 2 mM HPTS (pD = 12) (d).

3.2.1. Colorimetric ratiometric indicator displacement assay

Taking advantage of the significant difference in the pK_a values of the free HPTS dye and its AP6 complex, a colorimetric sensor has been constructed for the detection of nucleotide ATP. Adding ATP to a mixture of HPTS and AP6 with appropriate concentrations and pH, a decrease in the absorption band at 460 nm and an increase at 403 nm (Fig. 3. A, B), together with a fading of the bright green color (Fig. 3. C), has been observed. These changes are due to the displacement of deprotonated HPTS from its AP6 complex by ATP and the protonation of the dye once it is released.

The experimental conditions (pH and host concentration) were optimized to obtain maximum absorbance change at a selected ATP concentration (the details of the optimization process are presented in Section S3 of the SI). The optimal pH was found to be ≈ 7 (Fig. S2. A), which indicates that the sensor is ideal for applications under physiological conditions. The initial concentration of HPTS was taken as $2{\cdot}10^{-5}$ M, and the ideal AP6 concentration to achieve the largest absorbance change for the whole dynamic range was $1.5{\cdot}10^{-5}$ M (Fig. S2. B).

For the determination of the binding constant of ATP with AP6 (K_b), a solution of $2{\cdot}10^{-5}$ M HPTS was prepared in a 7 pH HEPES buffer, and AP6 was added in excess (2.1 equiv.). At this composition, only a negligible amount of 2:1 complex ($G_2{\cdot}M$) is formed, thus the total absorbance of the samples arises from the components G, G·M, GH·M and GH. A fitting to the absorption spectra (see Section S4 in the SI) yielded the value $K_b = 2.94{\cdot}10^{5}$ M^{-1}.

3.2.2. Fluorescent ratiometric indicator displacement assay

The same concept presented in Section 3.2.1. can be utilized in a fluorescent indicator displacement assay, as variations in the absorption spectra entail significant changes in fluorescent properties.

In the design of the fluorescent sensor, it has to be taken into consideration that the trianionic form of HPTS is a strong photoacid, in aqueous solution, the excited trianion dissociates before emission via a fast proton transfer to water molecules [38]. Thus, the steady-state emission band of trianionic HPTS coincides with the band of the tetraanionic species, but the fluorescence quantum yield of the trianionic form is lower. Therefore, applying the HPTS-AP6 supramolecular complex as a fluorescence sensor for ATP, two possible measurement methods are available: either the excitation wavelength is selected as 457 nm, the absorption maximum of the G·M form, and the emission spectra are recorded in the presence of ATP (Fig. 4. A), or the excitation spectra are recorded, and similarly to the colorimetric approach, a ratio of the intensities at 403 nm and 457 nm (the band maxima of the trianionic and tetraanionic forms of the dye) is used to calculate analyte concentration (Fig. 4. B).

Low $[G]_0$ and $[M]_0$ concentrations were selected to avoid the abundant formation of the 2:1 complex. Similarly to the colorimetric assay, the experimental conditions were optimized using the method presented in Section S3 of the SI.

The binding constant of ATP to AP6, K_b, was determined both from the emission and excitation spectra measured at different ATP concentrations by global fitting. The two values are presented in Table 2. The measured and fitted intensities at 515 nm and 457 nm are shown in Fig. 4. C. A limit of detection (LOD) of ≈ 1 μM was calculated by fitting of the initial linear responses in both the excitation and emission spectra.

The dynamic ranges of the FID assay for ATP, AMP, ADP and UTP are shown in Fig. 4. D, the binding constants for the complexes of these nucleotides with AP6 are presented in Table S1. None of the dynamic ranges of the other nucleotides overlap with that of ATP, and the K_b nucleotide·AP6 binding constant values obtained by fitting these titration curves are all more than an order of magnitude lower than for ATP.

The selectivity of the sensor was further investigated at 0.5 mM concentration of nucleotides ADP, AMP, GTP and UTP, tris(tetrabutylammonium) hydrogen pyrophosphate (PPi), natural amino acids L-Arginine, L-Lysine and L-Glutamic acid, as well as naturally occurring anions. Arginine and Lysine were selected because, as Kumar et al. previously demonstrated, HPTS undergoes deprotonation in the presence of basic amino acids [39], resulting in increased absorbance at 457 nm. In the context of the ATP sensor, this would lead to a negative error in the quantification of nucleotide concentration. A photograph of assay solutions containing selected nucleotides irradiated with a 460 nm LED is shown in Fig. 5. A. The fluorescence of the mixture containing the ATP analyte is turned off almost completely in contrast to the other samples. The bars in Fig. 5. B represent the ratios of the fluorescence excitation intensities measured at 403 nm and 457 nm in presence of analytes relative to the blank sample. Among the tested species, all nucleotides show some fluorescent responses, their magnitude following the order ATP > UTP > PPi > ADP > GTP > AMP. However, except for UTP, the responses induced by the competing nucleotides remained comparatively weak. The amino acids and the naturally occurring anions caused negligible fluorescent responses. The selectivity test was extended to

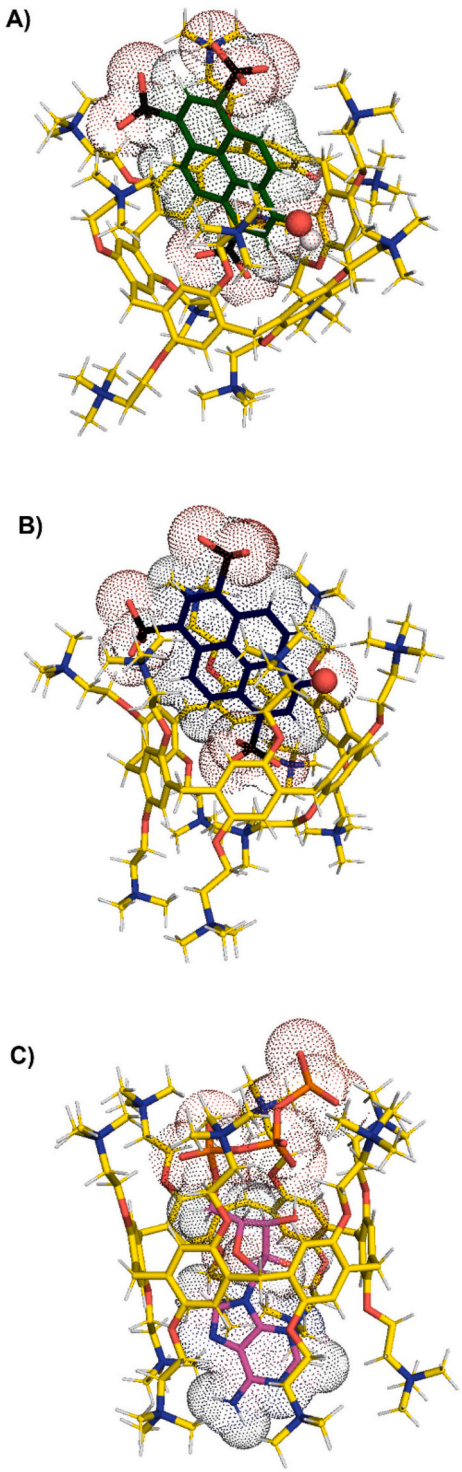

Fig. 7. Complex structures of protonated HPTS with AP6 (A), deprotonated HPTS with AP6 (B) and ATP with AP6 (C) based on DFT calculations.

common metal ions (Na^+, K^+, Ca^{2+}, Mg^{2+}, Fe^{3+}) and these ions also induced only minimal changes in the fluorescence signal (see Fig. S4. A).

We note that no significant changes were observed in the absorption, excitation and emission spectra of HPTS upon addition of the analytes in the absence of AP6.

3.2.3. Structures of the HPTS·AP6 and ATP·AP6 complexes

3.2.3.1. NMR spectra. The host-guest complexation of HPTS with cationic pillar[6]arene AP6 was investigated by ^1H NMR spectroscopy.

Comparison of the partial spectra of HPTS in Fig. 6 (a) and (d) reveals the structural effect of deprotonation. All proton signals shift upfield, consistent with increased electron-donation (M+) and enhanced shielding induced by the deprotonated hydroxyl group. This shift is most pronounced for proton **f**, located in the ortho position to the hydroxyl group.

In the 1:1 HPTS–AP6 mixtures, proton signals are broadened due to complexation dynamics. In both the protonated and deprotonated forms, proton **e** exhibits the most pronounced shift and broadening, indicating similar complex structures with partial or complete inclusion of the dye's aromatic core within the AP6 cavity. Most proton signals shift upfield, consistent with shielding by the electron-rich macrocyclic cavity. Exceptions are proton **a** in the protonated species and proton **f** in the deprotonated form, both of which display downfield shifts. These shifts can be attributed to local deshielding effects due to proximity to the electron-withdrawing trimethylammonium groups of the pillararene, or, in the case of proton **f**, to the attenuation of the shielding effect of the deprotonated hydroxyl group. These observations indicate subtle structural differences between the G·M and GH·M complexes.

A more detailed analysis of the titration series (0–2 equiv. AP6, Fig. S5. B and D) reveals a non-monotonic chemical shift trend for proton **f**. An initial upfield shift at 0.5 equiv. AP6 is followed by a reversal at higher host concentrations, which is consistent with a concentration-dependent equilibrium involving both 1:2 and 1:1 host–guest stoichiometries and corresponding structural rearrangements of the complexes.

The corresponding upfield region of the spectra, where the signals of the AP6 host are observed, is shown in Figs. S4. A and C. Upon complexation to both protonated and deprotonated HPTS, only minor upfield shifts of the AP6 signals with slightly larger shifts are observed for the binding of the deprotonated form. The most pronounced changes are observed for protons on the aromatic core and the methylene bridges of the macrocycle, consistent with partial or full inclusion of the guest.

The NMR spectrum of the ATP·AP6 complex has been previously investigated and reported in Ref. [28].

3.2.3.2. Theoretical calculations. For the interpretation of the structures predicted by NMR measurements and visualization of the complex structures, theoretical calculations have been performed.

The aromatic core of the HPTS dye is partially incorporated into the AP6 cavity in both the protonated and deprotonated HPTS complexes in a similar manner (Figs. 7. A and B). Protonated HPTS appears to be more deeply embedded within the cavity, inducing a more significant change in the macrocycle conformation. The differences observed in the NMR shifts of protons **a** and **f** in the complexes can be attributed to the distinct binding modes of the two guests.

Fig. 7. C shows the ATP·AP6 inclusion complex, held together by multiple strong interactions. The adenosine moiety fits inside the cavity of AP6, and its phosphate chain is long enough to form electrostatic interactions with the oppositely charged trimethylammonium groups [40].

The association energies of the complexes are given in Table S2. Since aqueous environments always give rise to specific interactions that are not fully accounted for in DFT calculations, these values should be considered only rough estimates, and the large difference between the GH·M and G·M binding constants cannot be rationalized on this basis. Nonetheless, ATP·AP6 complexes are consistently more stable than HPTS·AP6 complexes, suggesting that indicator displacement is expected to take place in these systems.

3.2.4. Turn-on hybrid fluorescent displacement sensor

rGO-AP6 is a nanocomposite assembled from reduced graphene oxide (rGO) and cationic ammonium pillar[6]arene (AP6). rGO-AP6 was synthesized and characterized previously by our research group [23]. In

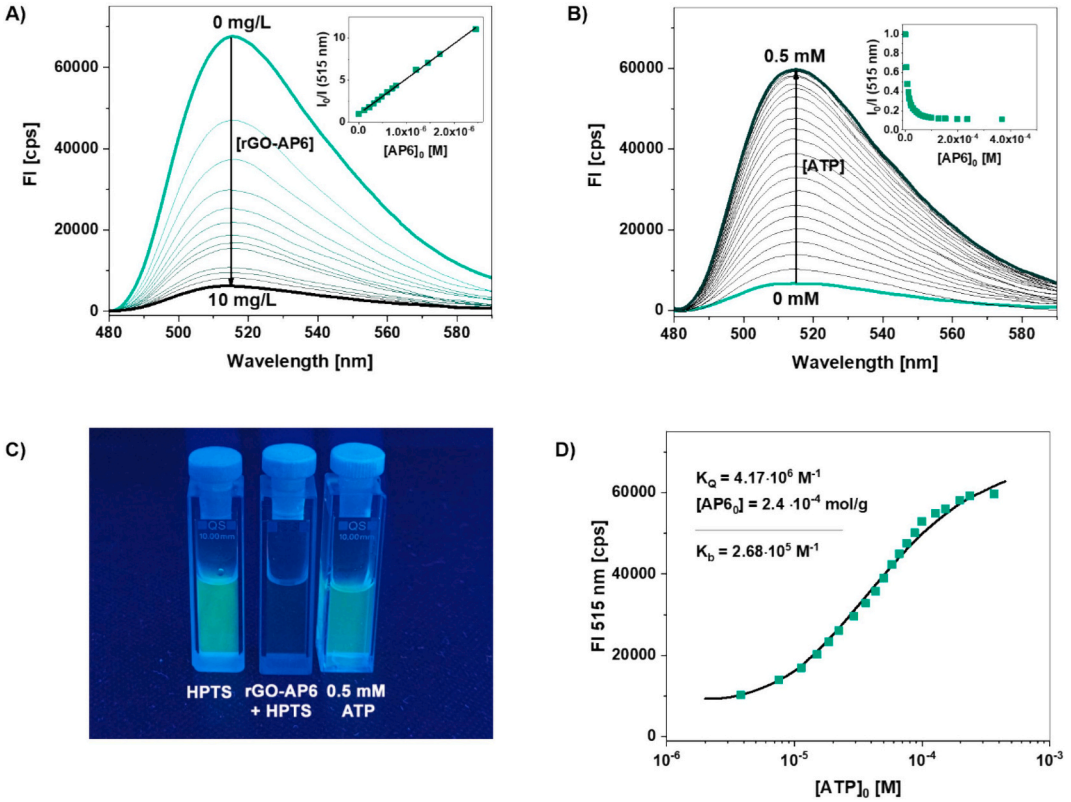

Fig. 8. (A) Emission spectra of HPTS ($5 \cdot 10^{-7}$ M) in the presence of 0–10 mg/l rGO-AP6, $\lambda_{exc} = 416$ nm; the inset shows the I_0/I ratios vs the concentration of AP6, (B) emission spectra of HPTS ($5 \cdot 10^{-7}$ M) + 10 mg/l rGO-AP6 in the presence of varying concentrations of ATP, $\lambda_{exc} = 416$ nm; (C) photographs of HPTS $5 \cdot 10^{-7}$ M, HPTS $5 \cdot 10^{-7}$ M + 10 mg/l rGO-AP6 and HPTS $5 \cdot 10^{-7}$ M + 10 mg/l rGO-AP6 + 0.5 mM ATP in HEPES buffer, 10 mM, pH = 7; (C) emission spectra of HPTS ($5 \cdot 10^{-7}$ M) + 10 mg/l rGO-AP6 in the presence of varying concentrations of ATP, $\lambda_{exc} = 416$ nm; (D) fluorescence intensity detected at 515 nm vs the initial concentration of ATP, semi-logarithmic scale; scattered plot – measured data, line plot – fitted models;

this work, utilizing the quenching effect of graphene oxide species, a *turn-on* FID-sensor for ATP based on FRET-effect has been constructed.

First, the quenching effect was examined using $5 \cdot 10^{-7}$ M HPTS solution in pH 7 HEPES buffer to which 10 mg/l rGO-AP6 was added. The sample was ultrasonicated intensely for 15 min. The dispersion was stable and no changes could be observed in its spectroscopic properties for ≈ 2 days. The emission spectra of HPTS in presence of increasing amounts of rGO-AP6 are shown in Fig. 8. A. From the XPS data published in [23], the maximum available concentration of AP6 binding sites on the surface of the nanocomposite is $2.4 \cdot 10^{-4}$ mol/g. The I_0/I ratios at the emission maximum were plotted against the AP6 concentration corresponding to the added rGO-AP6 composite, and fitted to a simple static quenching model [41].

$$\frac{I_0}{I} = K_Q[Q] + 1 \tag{5}$$

The binding constant of the rGO-AP6@HPTS system, taken as the quenching constant, K_Q obtained from this linear fit is $4.17 \cdot 10^6$ M^{-1}.

Subsequently, the HPTS solution with 10 mg/l rGO-AP6 was tested as an ATP sensor. At this nanocomposite concentration, the fluorescence is quenched almost completely. At the addition of 0–0.5 mM ATP, HPTS was displaced from the nanocomposite, and the emission of HPTS was regenerated (Fig. 8. B and C). At high ATP concentrations, a slight change in the excitation spectra and a decrease of the solution pH was observed, attributable to the acidity of ATP. To avoid the errors associated with the changes of the excitation spectra, the isosbestic point of the G and GH forms of HPTS (416 nm) was selected as the excitation wavelength.

The fluorescence intensities measured at 515 nm were fitted to a displacement model presented in Section S4. It was assumed that the detected emission is solely from free HPTS, and the HPTS molecules bound to rGO-AP6 are non-fluorescent. The binding constant K_b of the HPTS@rGO-AP6 complex in the presence of ATP was determined to be $2.68 \cdot 10^5$ M^{-1}, which is comparable to the values calculated for the HPTS·AP6 FID-system (Table 2). The LOD determined for the initial linear response of the sensor was 0.74 μM.

The association constants determined for the ATP·AP6 complex across the three experimental systems and detection methods are consistent with previously reported values (Yu et al. reported $1.52 \cdot 10^5$ M^{-1}, determined from isothermal titration calorimetry [28], whereas Bojtár et al. reported $4.45 \cdot 10^5$ M^{-1}, calculated from indicator displacement with fluorescent detection [40]). It should be noted that variations in ionic strength, pH and buffer composition might substantially affect the apparent binding constant.

The selectivity of the rGO-AP6@HPTS assay was evaluated against the same nucleotides, amino acids and anions as in case of the ratiometric fluorescent ATP sensor in Section 3.2.2. Fluorescence enhancement was measured at 515 nm in the presence of 0.5 mM of the analytes. Under 370 nm UV irradiation, the ATP-containing sample exhibited a markedly enhanced fluorescence compared to all other tested nucleotides (Fig. 9. A and B). The sensing ensemble also produced negligible response toward physiologically relevant metal ions (Fig. S4. B). Of the tested ions, Fe^{3+} caused a slight additional decrease of fluorescence, in agreement with the documented quenching of HPTS emission by transition metal ions [42].

It can be noted that in principle, our rGO-AP6 composite may be considered a nanosensor for the sequential *turn-off* and *turn-on* detection of HPTS dye and ATP. Recently, various nanosensors have been developed which are capable of the sequential detection of ionic analytes like the Ag/Au nanoclusters sensing sulfide and iodide [43] and sulfur-

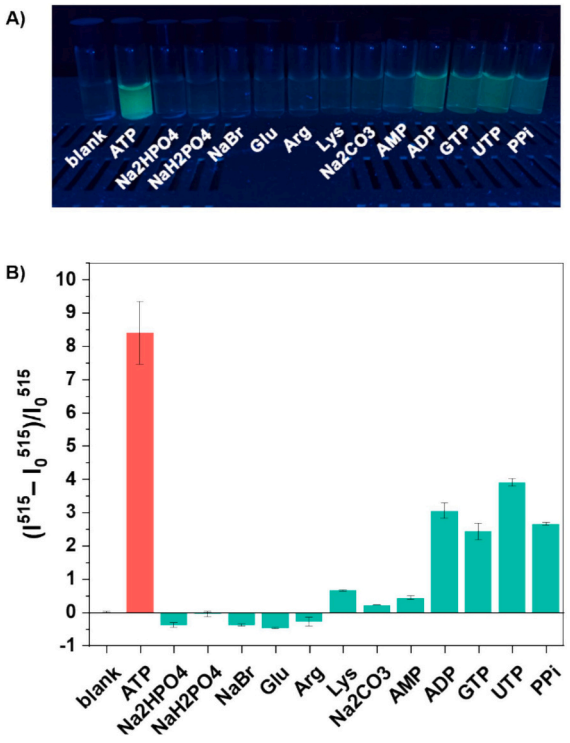

Fig. 9. (A) Photographs of the HPTS·rGO-AP6 assay in the presence of different analytes under 370 nm UV-light irradiation; (B) Fluorescence responses of the rGO-AP6·HPTS assay toward 0.5 mM ATP compared with nucleotides and amino acids (0.5 mM), $\lambda_{exc} = 416$ nm, $\lambda_{em} = 515$ nm, pH = 7; Error bars show standard errors of 3 parallel measurements.

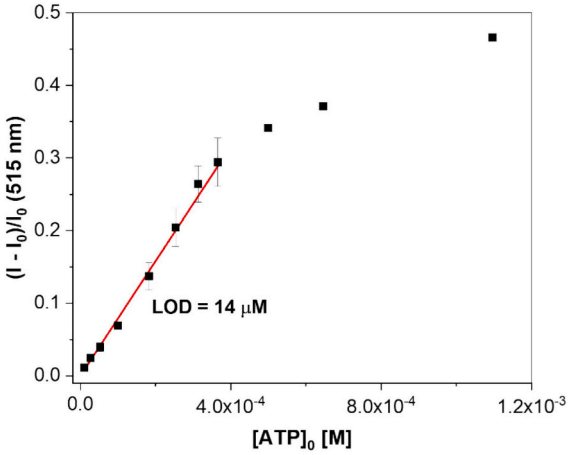

Fig. 10. Fluorescent response of the rGO-AP6@HPTS ($5{\cdot}10^{-7}$ M HPTS +10 mg/l rGO-AP6) indicator displacement sensor at 515 nm in the presence of varying concentrations of ATP (0–0.5 mM) in pH 7 HEPES buffer (10 mM) in the presence of 1% human serum.

functionalized carbon dots sensing aluminium and fluoride ions [44].

Inspecting the calibration curves in Fig. S3, the characteristics of the sensors operating with different detection modes can be compared. The LOD values for the three sensors with fluorescence detection fall in the range of 0.5–1.5 μM which is comparable to or better than those reported for related fluorescent ATP sensors [12,45]. The dynamic concentration range spans from ≈ 1 μM to ≈ 200 μM in case of all detection modes. In terms of its dynamic signal range, the FRET-type *turn-on* sensor is superior in performance, displaying a ≈ 10-fold maximal fluorescence enhancement upon ATP addition.

3.2.5. *Performance in human serum sample*

The applicability of the rGO-AP6@HPTS indicator displacement sensor in bioanalytical setting was assessed in the complex biological matrix of human serum. To a suspension of rGO-AP6 prepared in a solution of HPTS, 1 *w*/w% human serum was added. In the presence of ATP, the fluorescence of HPTS was regenerated. Due to the interference of biomolecules in the serum, a competition for the binding of HPTS occurred (see [46]), which resulted in a decrease of the apparent stability of the rGO-AP6·ATP complex ($\approx 2{\cdot}10^4$ M^{-1}) and an increase of the LOD (14 μM). On the other hand, a linear response was observed up to a higher ATP concentration ≈ 400 μM) (Fig. 10).

3.2.6. *Advantages, limitations and applicability of the assays*

The main advantage of the HPTS – AP6 system is its ratiometric detection mode, which is beneficial in experimental setups capable of simultaneously monitoring fluorescence intensities at two excitation wavelengths. Ratiometric assays provide robustness against fluctuations in probe concentration, background fluorescence, photobleaching or instrumental noise, making the assay suitable for biological systems characterized by relatively stable physiological pH (approximately 7) such as blood serum, plasma or cell lysates. The assay might also serve as a tool in live cell ATP imaging. Due to the cell-impermeability of its components [47,48], the ratiometric AP6–HPTS assay appears well suited for monitoring extracellular ATP. Its broad dynamic range and relatively low ATP-affinity make it an attractive tool for detection of high ATP concentrations released during purinergic signaling associated with high stress, damage, inflammation or cell death [49,50].

Association of the sensing ensemble with rGO is expected to alter its cellular localization by facilitating the intracellular delivery of the otherwise cell-impermeable components [51]. The rGO-AP6@HPTS sensor operates in *turn-on* mode, requires detection at a single emission wavelength or wavelength range. In terms of its fluorescence response range, this FRET-type *turn-on* sensor is superior in performance to the HPTS – AP6 assay, displaying a 9-fold relative fluorescence enhancement $(I - I_0)/I_0$ upon ATP addition. In human serum, the assay also displayed a broader dynamic range up to mM concentration range due to the interference of serum biomolecules that reduce the apparent ATP binding affinity. The assay might be advantageous for the quantification and imaging of cytosolic ATP, commonly in the millimolar concentration range.

4. Conclusions

In the present work, we have investigated the formation and characteristics of supramolecular complex AP6·HPTS. Our results demonstrate that cationic ammonium pillar[6]arene (AP6) preferentially binds the tetraanionic form of HPTS over its trianionic form, leading to a pronounced downward shift of the complex pK_a. This strong and selective protonation-state-dependent binding enables precise control over the dye's acid–base equilibrium within the host environment. This property can be exploited in a displacement assay in which HPTS is released from its AP6 complex in the presence of nucleotide ATP. Based on this concept, we designed both a colorimetric and a fluorescent ratiometric FID sensor with selectivity toward ATP over other nucleotides and pyrophosphate.

We have further examined the interaction of HPTS with AP6-functionalized reduced graphene oxide (rGO-AP6). The rGO-AP6 adduct also binds efficiently the indicator HPTS, but unlike pure AP6 pillararene host, it quenches the fluorescence of the dye via FRET effect. As tetraanionic HPTS is displaced from its rGO-AP6@HPTS complex by ATP, it is protonated to the trianionic form, restoring the fluorescence of free HPTS. This way, the rGO-AP6@HPTS complex functions as a *turn-on* FID assay for ATP.

The binding constants of the AP6·HPTS and rGO-AP6@HPTS complexes were found to be comparable, indicating that the surface immobilization of AP6 does not substantially alter its binding affinity toward

ATP. This highlights the robustness of the host–guest recognition motif upon nanomaterial integration, an important prerequisite for practical sensor design. The real life applicability of the rGO-AP6@HPTS sensor platform was demonstrated in human serum matrix.

These findings suggest that indicator displacement assays consisting of a fluorescent dye guest and a macrocyclic host grafted to a nanoparticle, the dye and the nanoparticle acting as a FRET pair, may be promising candidates for selective and sensitive nucleotide sensors with *turn-on* operation.

Funding sources

Financial support was obtained from the National Research, Development and Innovation (NRDI) Fund via research grants K143571 and Starting 152289. The work of D. Mester and E. Kovács was supported by the Bolyai János Research Scholarship of the Hungarian Academy of Sciences via research grants BO/00306/24 and BO/00085/24/7. E. Kiss gratefully acknowledges the support of the NRDI Office (research grant EKÖP-KDP-25-1-BME-19) and the research scholarship provided by ELTE Márton Áron Special College.

Declaration of competing interest

The authors declare that they have no known competing financial interests or personal relationships that could have appeared to influence the work reported in this paper.

Appendix A. Supplementary data

Supplementary data to this article can be found online at https://doi.org/10.1016/j.saa.2026.128536.

Data availability

Data will be made available on request.

References

[1] T.A. Johnson, H.A. Jinnah, N. Kamatani, Shortage of cellular ATP as a cause of diseases and strategies to enhance ATP, Front. Pharmacol. 10 (2019) 1–19, https://doi.org/10.3389/fphar.2019.00098.
[2] Y. Cao, E. Chen, X. Wang, J. Song, H. Zhang, X. Chen, An emerging master inducer and regulator for epithelial-mesenchymal transition and tumor metastasis: extracellular and intracellular ATP and its molecular functions and therapeutic potential, Cancer Cell Int. 23 (2023) 20, https://doi.org/10.1186/s12935-023-02859-0.
[3] H.F. Tzeng, C.H. Hung, J.Y. Wang, C.H. Chou, H.P. Hung, Simultaneous determination of adenosine and its metabolites by capillary electrophoresis as a rapid monitoring tool for 5′-nucleotidase activity, J. Chromatogr. A 1129 (2006) 149–152, https://doi.org/10.1016/j.chroma.2006.08.030.
[4] E. Sottofattori, M. Anzaldi, L. Ottonello, HPLC determination of adenosine in human synovial fluid, J. Pharm. Biomed. Anal. 24 (2001) 1143–1146, https://doi.org/10.1016/S0731-7085(00)00574-4.
[5] V.C. Özalp, L.J. Nielsen, L.F. Olsen, An aptamer-based nanobiosensor for real-time measurements of ATP dynamics, ChemBioChem 11 (2010) 2538–2541, https://doi.org/10.1002/cbic.201000500.
[6] D. Ji, H. Wang, J. Ge, L. Zhang, J. Li, D. Bai, J. Chen, Z. Li, Label-free and rapid detection of ATP based on structure switching of aptamers, Anal. Biochem. 526 (2017) 22–28, https://doi.org/10.1016/j.ab.2017.03.011.
[7] H.R. Tao, H. Yan, Z. Sun, Y. Bin Cui, N.B. Li, H.Q. Luo, A nanozipper structured efficient FRET probe for ratiometric detection of ATP based on target-induced cycling amplification, Sens. Actuators B Chem. 401 (2024) 134890, https://doi.org/10.1016/j.snb.2023.134890.
[8] L. Wang, Y. Huang, L. Sun, X. Gong, C. Dong, S. Shuang, A novel AIEgen-based probe integrated with split aptamer conjugates for adenosine triphosphate detection in beer, Spectrochim. Acta A Mol. Biomol. Spectrosc. 340 (2025) 126332, https://doi.org/10.1016/j.saa.2025.126332.
[9] G. Morciano, A.C. Sarti, S. Marchi, S. Missiroli, S. Falzoni, L. Raffaghello, V. Pistoia, C. Giorgi, F. Di Virgilio, P. Pinton, Use of luciferase probes to measure ATP in living cells and animals, Nat. Protoc. 12 (2017) 1542–1562, https://doi.org/10.1038/nprot.2017.052.
[10] Y. Wang, Y. Shen, J. Xue, L. Liu, Y. Li, Long-wavelength emissive N-doped carbon dots as a fluorescent probe for sensitive detection of pyrophosphate and cellular imaging, Spectrochim. Acta A Mol. Biomol. Spectrosc. 351 (2026) 127469, https://doi.org/10.1016/j.saa.2026.127469.
[11] N.C. Yang, W.M. Ho, Y.H. Chen, M.L. Hu, A convenient one-step extraction of cellular ATP using boiling water for the luciferin-luciferase assay of ATP, Anal. Biochem. 306 (2002) 323–327, https://doi.org/10.1006/abio.2002.5698.
[12] C. Zhang, G. Wu, Recent advances in fluorescent probes for ATP imaging, Talanta 279 (2024) 126622, https://doi.org/10.1016/j.talanta.2024.126622.
[13] Y.W. Jun, S. Sarkar, K.H. Kim, K.H. Ahn, Molecular probes for fluorescence imaging of ATP in cells and tissues, ChemPhotoChem 3 (2019) 214–219, https://doi.org/10.1002/cptc.201900001.
[14] J.B. Czirok, M. Bojtár, D. Hessz, P. Baranyai, L. Drahos, M. Kubinyi, I. Bitter, Aminonaphthalimide-based dipodal imidazolium/triazole receptors for fluorescent sensing of nucleoside polyphosphates, Sens. Actuators B-Chem. 182 (2013) 280–287, https://doi.org/10.1016/j.snb.2013.02.046.
[15] T. Deng, J. Chen, H. Yu, P. Yang, Y. Jian, G. Li, X. Zhou, H. Shen, J. Gui, Adenosine triphosphate-selective fluorescent turn-on response of a novel thiazole orange derivative via their cooperative co-assembly, Sens. Actuators B-Chem. 209 (2015) 735–743, https://doi.org/10.1016/j.snb.2014.12.008.
[16] P.P. Neelakandan, M. Hariharan, D. Ramaiah, A supramolecular ON-OFF-ON fluorescence assay for selective recognition of GTP, J. Am. Chem. Soc. 128 (2006) 11334–11335, https://doi.org/10.1021/ja062651m.
[17] X. Liu, H.T. Ngo, Z. Ge, S.J. Butler, K.A. Jolliffe, Tuning colourimetric indicator displacement assays for naked-eye sensing of pyrophosphate in aqueous media, Chem. Sci. 4 (2013) 1680–1686, https://doi.org/10.1039/c3sc22233k.
[18] X. Liu, D.G. Smith, K.A. Jolliffe, Are two better than one? Comparing intermolecular and intramolecular indicator displacement assays in pyrophosphate sensors, Chem. Commun. 52 (2016) 8463–8466, https://doi.org/10.1039/c6cc03680e.
[19] P.P. Neelakandan, M. Hariharan, D. Ramaiah, Synthesis of a novel cyclic donor-acceptor conjugate for selective recognition of ATP, Org. Lett. 7 (2005) 5765–5768, https://doi.org/10.1021/ol052246k.
[20] M. Shimizu, S. Aikawa, Y. Fukushima, Colorimetric detection of ATP by a Chlorophosphonazo III -based Mg2+ complex in aqueous solution via Indicator displacement approach, J. Fluoresc. 33 (2023) 255–260, https://doi.org/10.1007/s10895-022-03063-5.
[21] S. Mishra, S.M. Hossain, A.K. Singh, TICT fluorescent probe for Al3+: sequential detection of PPi, ATP and ADP in semi-aqueous medium and real-life applications, Spectrochim. Acta A Mol. Biomol. Spectrosc. 240 (2020) 118600, https://doi.org/10.1016/j.saa.2020.118600.
[22] W.C. Geng, Z. Ye, Z. Zheng, J. Gao, J.J. Li, M.R. Shah, L. Xiao, D.S. Guo, Supramolecular bioimaging through signal amplification by combining Indicator displacement assay with Förster resonance energy transfer, Angew. Chemie - Int. Ed. 60 (2021) 19614–19619, https://doi.org/10.1002/anie.202104358.
[23] E. Kiss, A. Bulátkó, J. Kozma, O. Krafcsik, M. Kubinyi, K. Kamarás, K. László, Binding characteristics of fluorescent probes to pillararene modified graphene oxide nanosheets and their implications for indicator displacement assays, Colloids Surfaces A Physicochem. Eng. Asp. 723 (2025) 137341, https://doi.org/10.1016/j.colsurfa.2025.137341.
[24] H. Imamura, K.P. Huynh, H. Togawa, K. Saito, R. Iino, Y. Kato-yamada, T. Nagai, H. Noji, Visualization of ATP levels inside single living cells with fluorescence resonance energy transfer-based genetically encoded indicators, PNAS 106 (2009) 15651–15656, https://doi.org/10.1073/pnas.0904764106.
[25] J.M. Conley, S. Radhakrishnan, S.A. Valentino, M. Tantama, Imaging extracellular ATP with a genetically-encoded, ratiometric fluorescent sensor, PloS One 12 (2017) e0187481., https://doi.org/10.1371/journal.pone.0187481.
[26] X. Cheng, Y. Cen, G. Xu, F. Wei, M. Shi, X. Xu, M. Sohail, Q. Hu, Aptamer based fluorometric determination of ATP by exploiting the FRET between carbon dots and graphene oxide, Microchim. Acta 185 (2018) 144, https://doi.org/10.1007/s00604-018-2683-z.
[27] W. Guo, Y. Wang, G. Qi, J. Wang, J. Ren, Y. Jin, E. Wang, Dual-signal readout sensing of ATP content in single dental pulp stem cells during differentiation via functionalized glass nanopipettes, Anal. Chim. Acta 1293 (2024) 342200, https://doi.org/10.1016/j.aca.2024.342200.
[28] G. Yu, J. Zhou, J. Shen, G. Tang, F. Huang, Cationic pillar[6]arene/ATP host-guest recognition: selectivity, inhibition of ATP hydrolysis, and application in multidrug resistance treatment, Chem. Sci. 7 (2016) 4073–4078, https://doi.org/10.1039/c6sc00531d.
[29] D.C. Marcano, D.V. Kosynkin, J.M. Berlin, A. Sinitskii, Z. Sun, A. Slesarev, L. B. Alemany, W. Lu, J.M. Tour, Improved synthesis of graphene oxide, ACS Nano 4 (2010) 4806–4814, https://doi.org/10.1021/nn1006368.
[30] I. Fekete-kertész, K. László, A. Bulátkó, B. Gyarmati, Z. Molnár, M. Molnár, Assessing the chronic environmental risk of graphene oxide using a multimarker approach across three trophic levels of the aquatic ecosystem, Nanomaterials 15 (2025) 1553, https://doi.org/10.3390/nano15201553.
[31] S. Tan, R. Han, S. Wu, H. Liang, Y. Zhao, H. Zhao, C.P. Li, A novel fluorescent sensing platform for insulin detection based on competitive recognition of cationic pillar[6]arene, Talanta 197 (2019) 130–137, https://doi.org/10.1016/j.talanta.2019.01.004.
[32] P. Pracht, S. Grimme, C. Bannwarth, F. Bohle, S. Ehlert, G. Feldmann, J. Gorges, M. Müller, T. Neudecker, C. Plett, S. Spicher, P. Steinbach, P.A. Wesołowski, Z. Felix, CREST—A program for the exploration of low-energy molecular chemical space, J. Chem. Phys. 160 (2024) 114110, https://doi.org/10.1063/5.0197592.
[33] C. Bannwarth, S. Ehlert, S. Grimme, GFN2-xTB - an accurate and broadly parametrized self-consistent tight-binding quantum chemical method with multipole electrostatics and density-dependent dispersion contributions, J. Chem. Theory Comput. 15 (2019) 1652–1671, https://doi.org/10.1021/acs.jctc.8b01176.

[34] J. Eberhardt, D. Santos-Martins, A.F. Tillack, S. Forli, AutoDock Vina 1.2.0: new docking methods, expanded force field, and Python bindings, J. Chem. Inf. Model. 61 (2021) 3891–3898, https://doi.org/10.1021/acs.jcim.1c00203.
[35] M.J. Frisch, et al., Gaussian 09, Gaussian Inc, Wallingford CT, 2009.
[36] J. Da Chai, M. Head-Gordon, Long-range corrected hybrid density functionals with damped atom-atom dispersion corrections, Phys. Chem. Chem. Phys. 10 (2008) 6615–6620, https://doi.org/10.1039/b810189b.
[37] P. Thordarson, Determining association constants from titration experiments in supramolecular chemistry, Chem. Soc. Rev. 40 (2011) 1305–1323, https://doi.org/10.1039/c0cs00062k.
[38] R. Nandi, N. Amdursky, The dual use of the Pyranine (HPTS) fluorescent probe: a ground-state pH Indicator and an excited-state proton transfer probe, Acc. Chem. Res. 55 (2022) 2728–2739, https://doi.org/10.1021/acs.accounts.2c00458.
[39] R.S. Bhosale, G.V. Shitre, R. Kumar, D.O. Biradar, S.V. Bhosale, R. Narayan, S. V. Bhosale, A 8-hydroxypyrene-1,3,6-trisulfonic acid trisodium salt (HPTS) based colorimetric and green turn-on fluorescent sensor for the detection of arginine and lysine in aqueous solution, Sens. Actuators B 241 (2017) 1270–1275, https://doi.org/10.1016/j.snb.2016.10.002.
[40] M. Bojtár, J. Kozma, Z. Szakács, D. Hessz, M. Kubinyi, I. Bitter, Pillararene-based fluorescent indicator displacement assay for the selective recognition of ATP, Sens. Actuators B 248 (2017) 305–310, https://doi.org/10.1016/j.snb.2017.03.163.
[41] D. Genovese, M. Cingolani, E. Rampazzo, L. Prodi, N. Zaccheroni, Static quenching upon adduct formation: a treatment without shortcuts and approximations, Chem. Soc. Rev. 50 (2021) 8414–8427, https://doi.org/10.1039/d1cs00422k.
[42] S. Biswas, S.C. Bhattacharya, S.P. Moulik, Quenching of fluorescence of 1-hydroxypyrene-3,6,8-trisulfonate (HPTS) by Cu2+, Co2+, Ni2+, I−, and cetylpyridinium (CP+) ions in water/AOT/heptane microemulsion, J. Colloid Interface Sci. 271 (2004) 157–162, https://doi.org/10.1016/j.jcis.2003.09.038.
[43] K. Wu, Y. Du, L. Yu, Y. Wang, S. Zhang, C. He, X. Li, J. Yao, M. Sun, S. Wang, Ligand-metal-metal charge transfer driven fluorescent au/ag nanoclusters for sensitive and selective detection of sulfide and iodide, Sens. Actuators B 466 (2026) 140324, https://doi.org/10.1016/j.snb.2026.140324.
[44] Q. Zhang, X. Li, L. Yu, L. Wang, Z. Wen, P. Su, Z. Sun, S. Wang, Machine learning-assisted fluorescence visualization for sequential quantitative detection of aluminum and fluoride ions, J. Environ. Sci. 149 (2025) 68–78, https://doi.org/10.1016/j.jes.2024.01.023.
[45] Y. Zhang, R. Miao, W. Ma, H. Sha, H. Chen, A dual-emission ZIF-based AIE nanoprobe for ratiometric fluorescence combined with colorimetric detection of ATP, Sens. Actuators B 447 (2026) 138834, https://doi.org/10.1016/j.snb.2025.138834.
[46] B. Cohen, C. Martin Álvarez, N. Alarcos Carmona, J.A. Organero, A. Douhal, Proton-transfer reaction dynamics within the human serum albumin protein, J. Phys. Chem. B 115 (2011) 7637–7647, https://doi.org/10.1021/jp200294q.
[47] M.T.Z.. Spence, I.D. Johnson, Probes useful at near-neutral pH—Section 20.2., in: Mol. Probes Handb. A Guid. To Fluoresc. Probes Labeling Technol., 11th ed., Life Technogies Corporation, Carlsbad, CA, 2010.
[48] C.-P. Li, Y.-X. Lu, C.-T. Zi, Y.-T. Zhao, H. Zhao, Y.-P. Zhang, Cationic pillar[6]arene induces cell apoptosis by inhibiting protein tyrosine phosphorylation via host–guest recognition, Int. J. Mol. Sci. 21 (2020) 4979, https://doi.org/10.3390/ijms21144979.
[49] L. Hua, J. Emily, S.P. Muench, S. Roger, Structural basis for the functional properties of the P2X7 receptor for extracellular ATP, Purinergic Signal. 17 (2021) 331–344, https://doi.org/10.1007/s11302-021-09790-x.
[50] V. Vultaggio-poma, A.C. Sarti, F. Di Virgilio, Extracellular ATP: a feasible target for Cancer therapy, Cells 9 (2020) 2496, https://doi.org/10.3390/cells9112496.
[51] X. Mao, T. Liu, J. Bi, L. Luo, D. Tian, H. Li, The synthesis of pillar[5]arene functionalized graphene as a fluorescent probe for paraquat in living cells and mice, Chem. Commun. 52 (2016) 4385–4388, https://doi.org/10.1039/c6cc00949b.